

# Maximal chromosome compaction occurs by axial shortening in anaphase and depends on Aurora kinase

Felipe Mora-Bermúdez<sup>1</sup>, Daniel Gerlich<sup>1,2</sup> and Jan Ellenberg<sup>1,3</sup>

**Eukaryotic cells must first compact their chromosomes before faithfully segregating them during cell division. Failure to do so can lead to segregation defects with pathological consequences, such as aneuploidy and cancer<sup>1,2</sup>. Duplicated interphase chromosomes are, therefore, reorganized into tight rods before being separated and directed to the newly forming daughter cells<sup>3</sup>. This vital reorganization of chromatin remains poorly understood. To address the dynamics of mitotic condensation of single chromosomes in intact cells, we developed quantitative assays based on confocal time-lapse microscopy of live mammalian cells stably expressing fluorescently tagged core histones. Surprisingly, maximal compaction was not reached in metaphase, but in late anaphase, after sister chromatid segregation. We show that anaphase compaction proceeds by a mechanism of axial shortening of the chromatid arms from telomere to centromere. Chromatid axial shortening was not affected in condensin-depleted cells, but depended instead on dynamic microtubules and Aurora kinase. Acute perturbation of this compaction resulted in failure to rescue segregation defects and in multilobed daughter nuclei, suggesting functions in chromosome segregation and nuclear architecture.**

The structural changes that underlie the compaction of mitotic chromosomes are naturally dynamic. However, only a few studies have quantified compaction in live cells, and none has investigated all mitotic stages. Also, several molecular players involved in chromosome compaction have been extensively studied<sup>3</sup>, but the activities directly responsible for the dynamic compaction *in vivo* remain elusive. A kinetic understanding of the compaction process is, therefore, missing. In living *Drosophila* embryos, chromatin was shown to be more compact in metaphase than in prophase or telophase<sup>4</sup>, and decompaction was shown to be anisometric, with dense peripheral foci decompacting slower than less dense central chromatin<sup>5,6</sup>. Observations consistent with this were made in mammalian cells<sup>7</sup>. In early mitosis, total chromatin density was shown to increase in prophase and prometaphase<sup>8</sup>.

However, individual chromosome widths change little during prometaphase<sup>9</sup>. This suggests that intrachromosome compaction is completed in prophase and only interchromosome proximity increases further during congression in prometaphase.

With few exceptions, most compaction studies have focused on pre-segregation events. It is, however, during anaphase that the critical function of mitotic chromosome compaction becomes most evident. Compact anaphase chromosomes are essential for segregation and reduce the risk of chromatin damage when the cytokinetic furrow splits the cell, especially in organisms with long chromosomes, such as humans<sup>3</sup>.

During anaphase in budding yeast, a Cdc14–condensin-dependent chromatid resolution and axial shortening was shown to participate in the segregation of the rDNA locus<sup>10</sup>, which also involves Aurora B phosphorylation of condensins<sup>11,12</sup>. Interestingly, this proceeded without microtubules<sup>13</sup>, suggesting the existence of segregation forces other than the mitotic spindle.

To investigate the overall kinetics of mitotic chromosome compaction, we first measured the volume occupied by all chromatin in NRK cells stably expressing EGFP-tagged histone 2B (EGFP–H2B) by four-dimensional imaging from G2 to telophase (Fig. 1a and see Supplementary Information, Movie S1). As expected, the measured volume remained constant during G2 and decreased markedly during prophase and prometaphase until metaphase (Fig. 1b). This volume increased during segregation in early anaphase, leading to a transient dip in apparent compaction. Surprisingly, after segregation and before telophase decompaction, the volume decreased to the lowest level, suggesting that chromatin reached maximal compaction ~8–12 min after anaphase onset (Fig. 1b). Afterwards, chromatin decompactes during telophase as expected. From interphase to mitosis, the measured chromatin volume decreased only ~2–3-fold. However, important changes in chromatin structure occur below the resolution of four-dimensional live-cell imaging and thus, may be underestimated by this assay.

The volumetric assay could not distinguish whether the minimal chromatin volume in late anaphase resulted from compaction of individual chromosomes or increased proximity between different

<sup>1</sup>Gene Expression and Cell Biology/Biophysics Units, European Molecular Biology Laboratory, Meyerhofstr. 1, 69117 Heidelberg, Germany. <sup>2</sup>Current address: Institute of Biochemistry, Schafmattstrasse 18 ETH-Hönggerberg, HPM E17.2 CH-8093, Zürich, Switzerland.

<sup>3</sup>Correspondence should be addressed to J.E. (e-mail: jan.ellenberg@embl.de)

Received 29 January 2007; accepted 14 May 2007; published online 10 June 2007; DOI: 10.1038/ncb1606

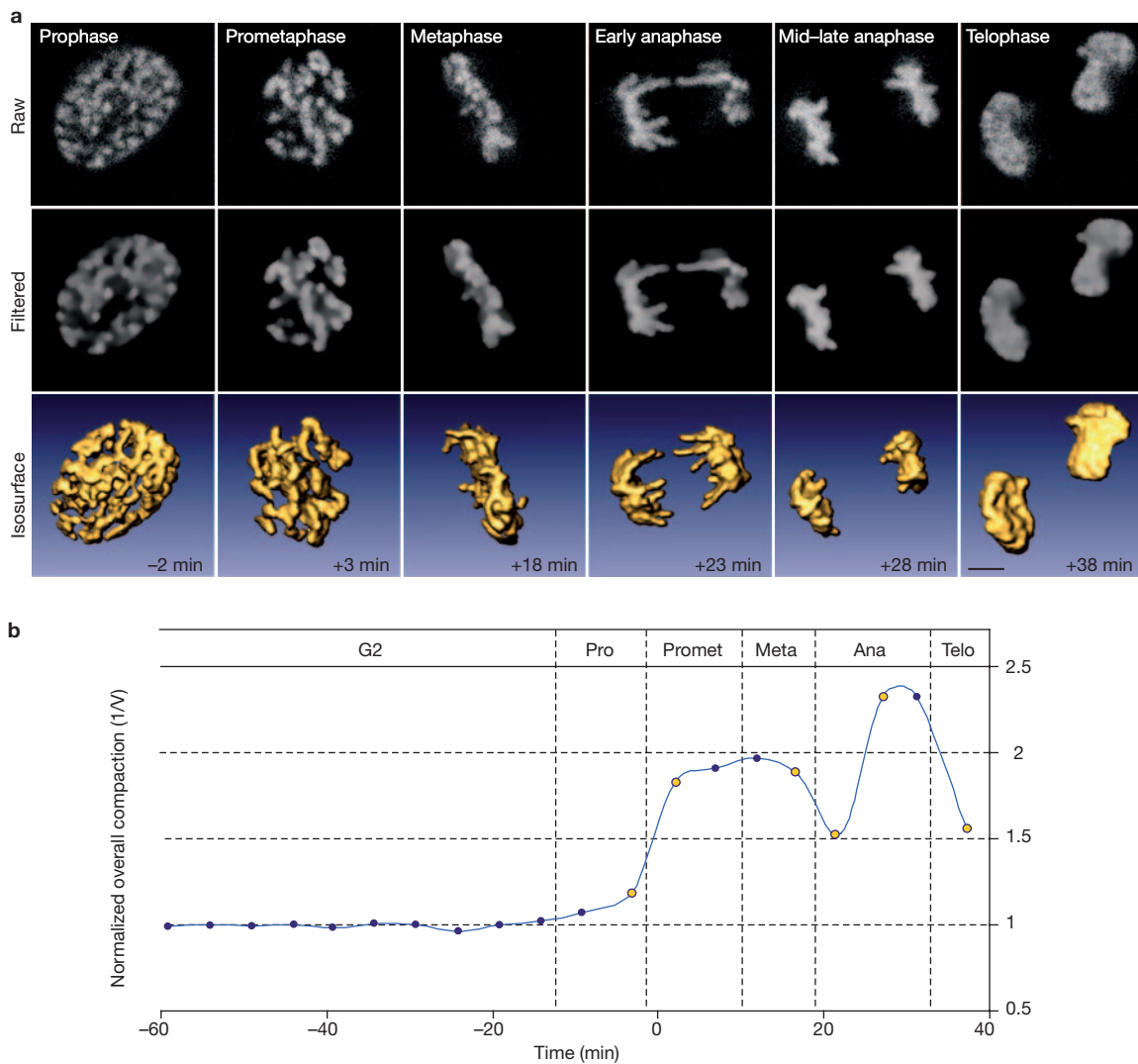


**Figure 1** Large-scale chromatin compaction in late anaphase. Changes in the volume occupied by chromatin through mitosis, quantified in a monoclonal NRK cell line stably expressing EGFP-H2B. **(a)** Using in-house developed macros, the raw fluorescence signal of all single confocal sections was filtered and used to calculate the volume occupied by chromatin over time (bottom; see Supplementary Information, Methods). The scale bar represents 5  $\mu$ m. **(b)** Chromatin compaction, defined as the inverse of its volume, plotted over

time (representative cell of  $n = 10$  cells from four independent experiments). For experiments with higher temporal resolution, see Supplementary Information, Fig. S5. Compaction was normalized to the G2 chromatin volume.  $t = 0$  was at chromosome congression onset; time lapse was 5 min. Vertical dotted lines indicate the approximate transitions between cell cycle phases (pro, prophase; promet, prometaphase; meta, metaphase; ana, anaphase; telo, telophase). Yellow dots in the curve correspond to the images in **a**.

chromosomes (see Supplementary Information, Methods). To determine whether individual chromosomes compacted further in anaphase, single chromosome segments were followed by photoactivation from prometaphase throughout mitosis (Fig. 2a, b). Chromosome segment length, and mean and total fluorescence intensities were measured to monitor compaction (see Methods). These parameters remained similar from prometaphase to anaphase onset, confirming that little or no intrachromosome compaction occurs during prometaphase and metaphase (Fig. 2b and ref. 9). In addition, the combined total fluorescence intensity of the two sister chromatids remained constant throughout mitosis, ruling out histone dissociation or photobleaching effects (Fig. 2c). In contrast, during mid-anaphase, the lengths of chromatid segments decreased, coupled to a simultaneous increase in their mean intensity that reached an overall maximum ~8–10 min post-anaphase onset. Therefore, single chromatid

compaction reaches its maximum in late anaphase. Later, the segment lengths increased and the mean intensities decreased, as expected during telophase decompaction.

To confirm an axial shortening along the total length of chromatid arms between telomere and centromere in anaphase, chromosomes were imaged with differentially labelled arms and pericentromeric heterochromatin (see Supplementary Information, Fig. S1). When segregation was completed (~2 min post-anaphase onset) and before telophase decondensation, chromosome arms that protruded from the chromatin mass of sub-centromeric regions at the spindle poles, reduced their initial length by about half after ~8–12 min, consistent with the photoactivation results in Fig. 2b (see also Supplementary Information, Movie S2).

Taken together, these assays show that chromosome arms compact by axial shortening after sister-telomere separation in anaphase.

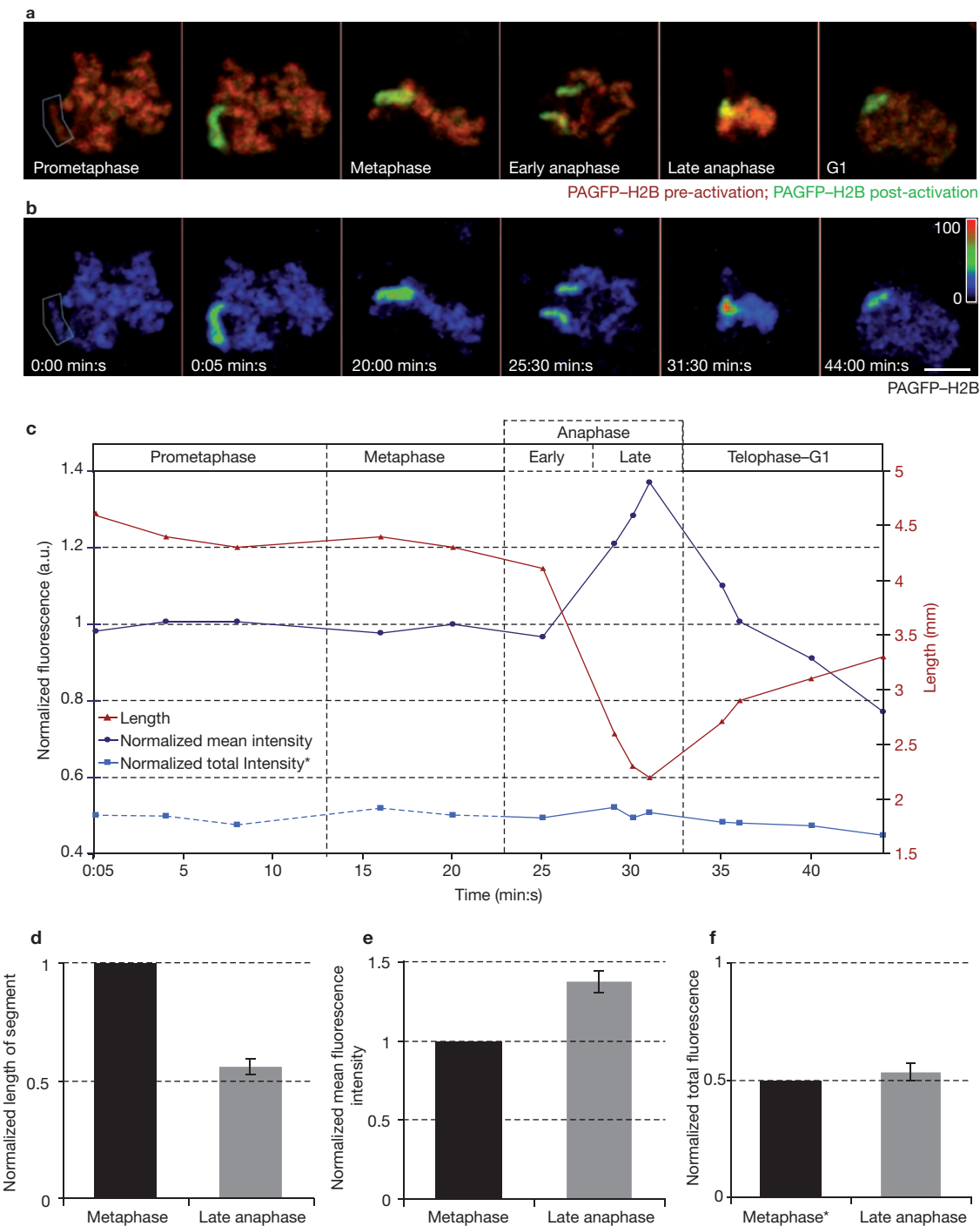


**Figure 2** Anaphase chromosome compaction by chromatid axial shortening. **(a, b)** Mean intensity projections of two confocal sections of a representative NRK cell stably expressing photoactivatable GFP-tagged H2B (H2B-PAGFP), giving a combined field width half maximum of 1.5  $\mu\text{m}$ . Merge of the photoactivated (green) and non-photoactivated (red) channel is shown in **a**. Photoactivated channel in pseudocolour with intensities according to the colour scale is shown in **b**. During congression and alignment on the metaphase plate, distinct large segments ( $\leq 5 \mu\text{m}$  long) in single chromosomes that became transiently spatially isolated from the rest in three dimensions were labelled by photoactivation with a short 405 or 413 nm laser pulse (blue polygon at  $t = 0:00$ ). The scale bar represents 5  $\mu\text{m}$ .

**(c)** Quantification of the length (red), mean fluorescence intensity (dark blue), and total fluorescence intensity (light blue) of the single labelled segment in **a** through mitosis. Fluorescence intensities were normalized to the last metaphase value ( $t = 20:00$ ). For clarity, the total intensity of replicated chromosomes up to the last metaphase value was divided by two to better compare with the values of single chromatids after anaphase segregation (dashed line and asterisk in **c** and asterisk in **f**). **(d-f)** Mean and standard deviation for all segment lengths **(d)**, mean fluorescence intensities **(e)** and total fluorescence intensities **(f)** in late anaphase, normalized to metaphase. Measurements in **c-f** were on the unprojected single sections ( $n = 10$  segments and cells in eight independent experiments).

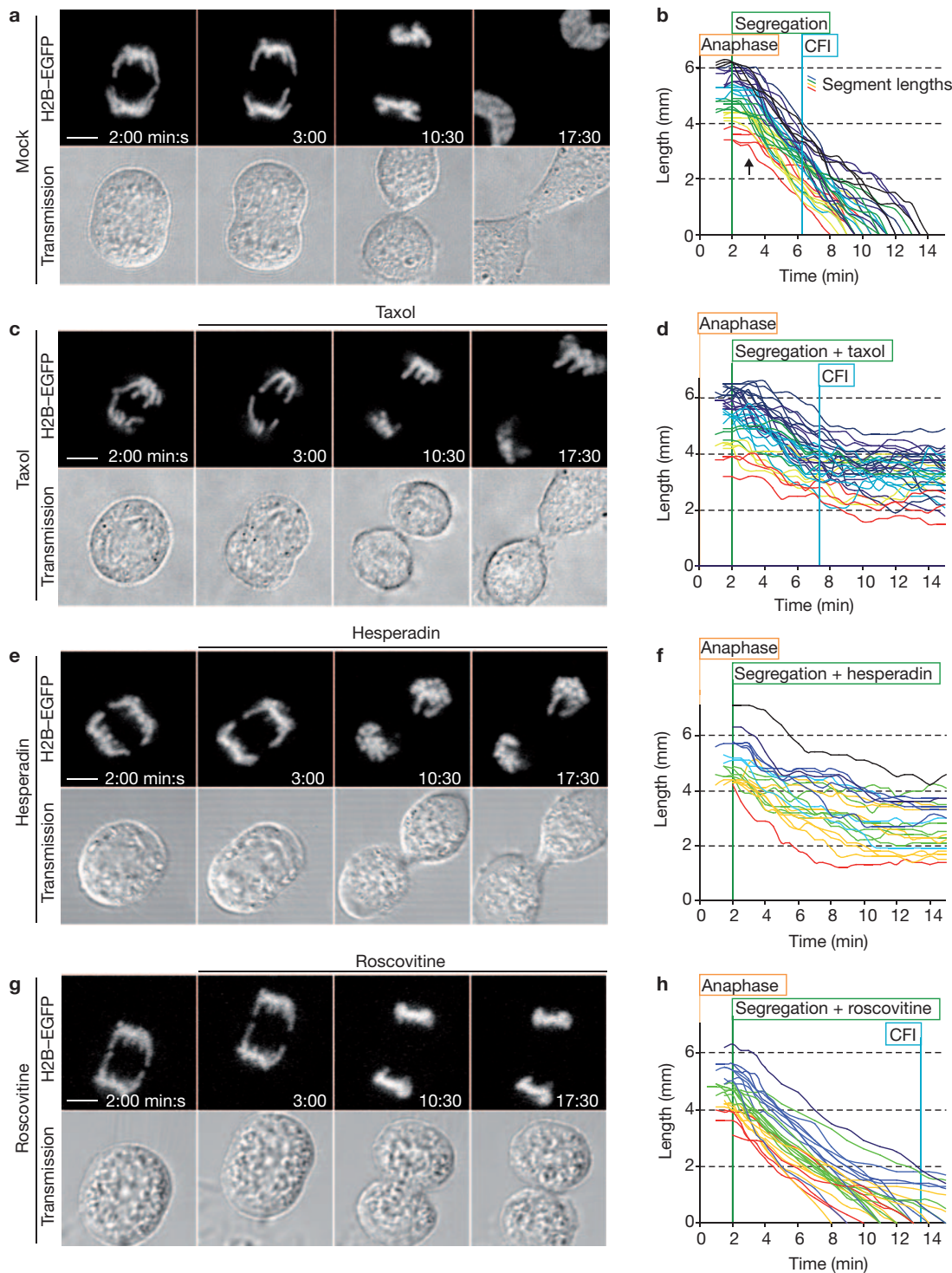


**Figure 3** Anaphase chromatid arm shortening requires dynamic microtubules and active Aurora B. Single confocal sections and transmission images from time-lapse recordings of the same NRK cell line expressing EGFP-H2B as in Fig. 1. The lengths of protruding chromatid arms were measured as described in Supplementary Information, Fig. S1a. Microtubule-perturbing drugs were applied as described in the Supplementary Information, Fig. S2. (a) Mock-treated cell. (b) Quantification of 34 chromatid segment shortenings in 15 independently mock-treated cells; CFI is full cleavage

furrow ingression. (c) Taxol-treated cell. (d) Quantification of 36 chromatid segment shortenings in 15 independently taxol-treated cells. (e) Hesperadin-treated cell. (f) Quantification of 23 chromatid segment shortenings in 10 independently hesperadin-treated cells. (g) Roscovitine-treated cell. (h) Quantification of 30 chromatid segment shortenings in 12 independently roscovitine-treated cells. Colours indicate initial lengths of chromatid segments (red: short, to dark blue: long). The moment of addition of small molecule inhibitors is indicated. The scale bars represent 5  $\mu$ m.

Furthermore, the consistent results between entire chromatid arms and large labelled segments indicate that arm segments are faithful reporters of chromatid-arm compaction.

Consequently, the global chromatin marker H2B-EGFP was used to measure the shortening kinetics of protruding segments from anaphase to telophase (Fig. 3a and see Supplementary Information, Fig. S1 and Movie S3). Chromosome arms shortened away from the central spindle and cytokinesis plane with a generally constant rate of  $0.6 \pm 0.1 \mu\text{m min}^{-1}$ , starting after poleward migration of sub-centromeric chromatin masses was  $\sim 90\%$  complete. In contrast, the rate of poleward separation of chromatin masses was six times higher ( $3.6 \pm 0.5 \mu\text{m min}^{-1}$ ), exhibited plateauing kinetics at the onset of arm retraction and stopped  $\sim 4$  min after anaphase onset, when shortening had proceeded by only one fifth (see Supplementary Information, Fig. S1). Chromosome-arm compaction is thus kinetically distinct and temporally independent of the spindle-mediated poleward separation of chromatin masses. Furthermore, arm compaction was not significantly affected when cleavage furrow ingressoin (CFI) was fully inhibited by the actin-depolymerizing drug latrunculin (see Supplementary Information, Fig. S3e, f). Shortening occurred with slow, linear kinetics, and initiated either more slowly than its eventual mean rate or started altogether after a delay of up to 1.5 min after telomere separation (Fig. 3b). The kinetics of axial shortening are thus inconsistent with a spring-like elastic recoil of chromosomes after segregation, but support a progressive axial compaction.

Axial shortening could be caused by chromatin-intrinsic forces or by forces involving microtubules. We have shown that this shortening is temporally independent of the poleward pulling of chromosomes by the kinetochore fibres (K-fibres). However, dynamic anaphase microtubules also form the midspindle. To determine whether such microtubules were required, it was crucial to perturb them acutely and rapidly within the  $\sim 10$ – $15$  min duration of anaphase, without affecting K-fibre-driven chromosome segregation in early anaphase. Therefore, the action kinetics of the microtubule-perturbing drugs taxol and nocodazole were first measured in live anaphases, showing that a strong perturbation could be achieved within 2 min of drug addition (see Supplementary Information, Fig. S2).

Next, the anaphase-shortening kinetics were quantified in mock-treated control cells, where all 34 measured chromatids, typically representing late-segregating chromosomes, shortened completely within 14 min post-anaphase onset (Fig. 3a, b). In contrast, acute taxol treatment at the moment of separation of the last telomere pair in early anaphase impaired shortening in all 36 measured chromatid arms (Fig. 3c, d and see Supplementary Information, Movie S4). Consistent results were obtained in cells where microtubules were acutely depolymerized by nocodazole (29 of 36 measured arms (81%) failed to fully shorten within 15 min; see Supplementary Information, Fig. S3). Thus, dynamic microtubules are required for the axial shortening of chromatid arms in anaphase.

Because chromatid shortening continued after completion of the poleward migration of chromatin masses, we hypothesized that a functional midspindle, rather than dynamic microtubules *per se*, could be required. To test this hypothesis, an essential midspindle component, Aurora B kinase, was acutely inhibited by applying the specific small molecule inhibitor hesperadin<sup>14</sup>. Similar to the microtubule perturbations, all 23 measured chromosome arms failed to shorten normally (Fig. 3e, f), whereas the structure of the early anaphase spindle was

unaffected (see Supplementary Information, Fig. S2). Consistent results were obtained in cells treated with ZM447439, a structurally different specific Aurora kinase inhibitor<sup>15</sup> (see Supplementary Information, Fig. S3). As a negative control, the effect of roscovitine was examined — a potent inhibitor of cyclin-dependent kinases (CDKs), whose activity is required for several mitotic events<sup>16</sup>, and has been linked to mitotic chromosome structure<sup>17</sup>. In contrast with the Aurora inhibitors, even at very high concentrations of roscovitine (360  $\mu\text{M}$ ; see Supplementary Information, Fig. S4), most measured chromatids (22 of 30; 73%) shortened normally in anaphase (Fig. 3g, h). Aurora kinase activity is therefore required for anaphase chromatid shortening.

When the shortening was perturbed by either microtubule or Aurora inhibition, abnormal multilobed nuclei were formed instead of the smooth ellipsoid nuclei observed in control experiments. Each lobe could be tracked back to an incompletely compacted anaphase chromatid in the four-dimensional data sets (Fig. 3c–e, and see Supplementary Information, Fig. S5 and Movie S4). This strongly suggests that anaphase shortening is required for the formation of smooth nuclei with normal chromatin architecture after mitosis. Finally, Aurora B depletion by RNAi results in hypomorphic mitotic phenotypes that also exhibit multilobed daughter nuclei, consistent with a dependence of chromosome shortenings on Aurora B (ref. 18; Neumann, B., F. M. -B. and J. E., unpublished observations).

The negative effect of microtubule poisons on anaphase shortening could be exerted indirectly by perturbing Aurora B. To examine this possibility, Aurora B localization was analysed by immunofluorescence microscopy after acute microtubule perturbation. In early anaphase of mock-treated cells, the localization of Aurora B was intermediate between the kinetochore localization in metaphase and the equatorial plane in late anaphase. In mid-anaphase Aurora B localized exclusively to a thin equatorial band, consistent with the expected midspindle localization (Fig. 4a). In cells pretreated with taxol for 8 min before fixation, Aurora B localized normally from prophase to metaphase. In anaphase, however, it was diffusely distributed in a striped pattern between the chromatin masses, and was not enriched in the equatorial plane (Fig. 4b). Consistently, in cells pretreated with nocodazole, Aurora B was diffusely localized on anaphase chromatin, not enriched in the equatorial plane (Fig. 4c). Thus, dynamic microtubules are required for the correct localization of Aurora B during anaphase. This is consistent with the view that microtubule perturbations inhibit chromosome shortening by displacing Aurora B from its physiological site of action.

Aurora B and condensins have been shown to participate in a Cdc14-dependent axial shortening of rDNA loci in budding yeast during anaphase<sup>10–12</sup>, and we have previously shown that condensin I is enriched in chromosomes during anaphase in mammalian cells<sup>9</sup>. Therefore, condensins were a strong chromatin-intrinsic candidate to mediate anaphase compaction. To investigate this possibility, RNA interference (RNAi) was used to deplete the SMC2 subunit that is essential for functional condensin I and II complexes. Cells transfected with non-silencing control siRNA (scrambled) showed shortening kinetics similar to NRK cells (Figs. 3a, b and 5a, b). On the other hand, SMC2-depleted cells showed the characteristic phenotype<sup>9</sup> of massive segregation problems and slower early anaphase kinetics, probably caused by anaphase bridges. Nevertheless, most detected chromosome bridges finally resolved during mid-late anaphase and eventually managed to fully shorten with rates similar to controls (Fig. 5c, d). This strongly suggests that condensins

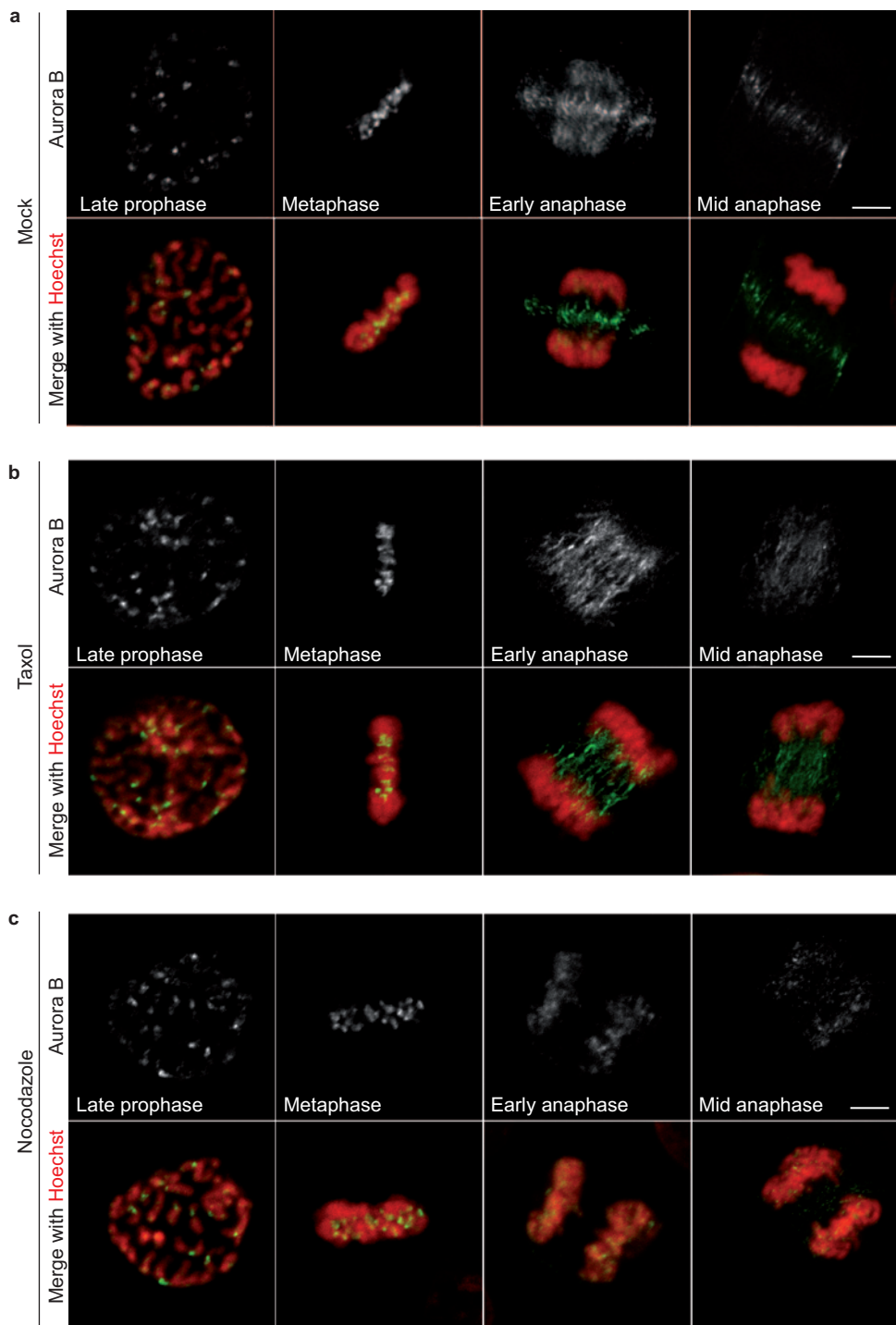


**Figure 4** Midspindle localization of Aurora B in early anaphase requires dynamic microtubules. Single confocal sections of fixed HeLa cells stained for Aurora B (green) and DNA (red). Mitotic stages were determined from the chromosome morphology, and the entire cell in transmission images (data not shown).

Representative cells ( $n \geq 15$  for each mitotic stage and treatment) from two independent experiments each. (a–c) Control cells treated with the drug solvent DMSO (a), cells treated with 20  $\mu$ M taxol (b) and cells treated with 20  $\mu$ M nocodazole (c), each for 8 min before fixation. The scale bars represent 5  $\mu$ m.

are not required for anaphase shortening. Furthermore, four anaphase bridges were observed that resolved and shortened after completion of the spindle-mediated poleward movement of chromatin masses (Fig. 5c). This indicated that mechanisms other than poleward pulling of centromeres were mediating the late resolution of bridged chromosomes.

Anaphase chromatid shortening could function as such a rescue mechanism for chromosome segregation defects. To examine this possibility, the same condensin-depleted cells were used as a system with a high frequency of early anaphase segregation defects. In these cells, arm shortening was acutely inhibited by adding taxol when the poleward

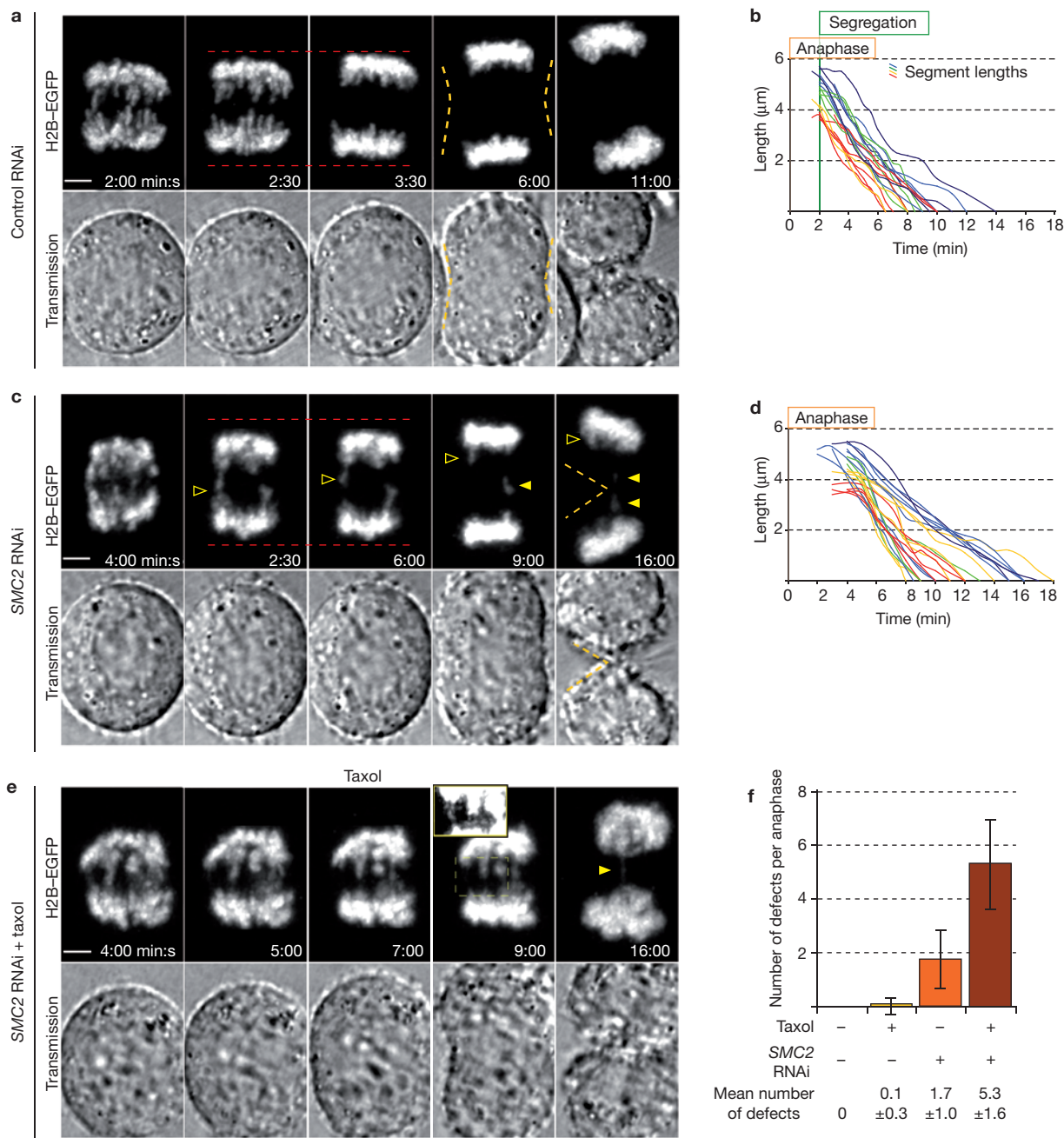


**Figure 5** Resolution of segregation defects in *condensin*-depleted cells depends on dynamic anaphase microtubules. Confocal sections and transmission images of HeLa cells stably expressing H2B-EGFP. (a) Mock-treated mock-depleted cell; yellow dashed lines highlight the onset of cleavage furrow ingression (CFI). (b) Length of 20 chromatid segments over time in 14 independently mock-treated mock-depleted cells. (c) Mock-treated SMC2-depleted cell. A bridged anaphase chromosome ( $t = 5:30$ , open arrow head) resolves and incorporates into chromatin masses ( $t = 6:00–16:00$ ) after completion of poleward movement of chromatin masses (compare red horizontal dashed lines at  $t = 5:30$  and  $t = 6:00$  min). (d) Length of 23 chromatid segments in mock-treated SMC2-depleted cells. (e) Taxol-treated SMC2-depleted cell. Five detected segregation defects persist at onset of CFI (see magnification of projected z-stack, with four contiguous defects), and one detected bridge remained unresolved even after complete CFI. (f) Mean number of detected segregation defects per cell at the onset of CFI. The scale bars represent 5  $\mu\text{m}$ .

motion of the chromatin masses had largely ceased. Then, the remaining segregation defects were counted at the first sign of CFI (Fig. 5a, 6 min). In 14 mock-treated/mock-depleted cells, no segregation defects were detected. Similarly, in taxol-treated/mock-depleted cells, one defect in

s). The increase distance thereafter resulted from CFI. Only the length of chromatids segregated before CFI onset were measured; closed arrow head highlights a segregation defect not rescued where the chromosome is eventually cut in two unequal fragments by the cleavage furrow. (d) Length of 23 chromatid segments in mock-treated SMC2-depleted cells. (e) Taxol-treated SMC2-depleted cell. Five detected segregation defects persist at onset of CFI (see magnification of projected z-stack, with four contiguous defects), and one detected bridge remained unresolved even after complete CFI. (f) Mean number of detected segregation defects per cell at the onset of CFI. The scale bars represent 5  $\mu\text{m}$ .

13 cells was detected. In 17 mock-treated SMC2-depleted cells,  $1.7 \pm 1.0$  segregation defects per cell were observed that could not be resolved before cleavage onset (Fig. 5c), consistent with previous observations<sup>9</sup>. In 14 taxol-treated SMC2-depleted cells, an average of  $5.3 \pm 1.6$

segregation defects were counted, a more than threefold statistically significant increase compared to mock-treated *condensin*-depleted cells (*t*-test,  $P = 2.59 \times 10^{-7}$ ; Fig. 5f). Thus, acute perturbation of dynamic microtubules in anaphase not only inhibits chromosome shortening, but also prevents the resolution of chromosome bridges induced by *condensin* depletion.

The current view of chromatin compaction is that the most compact state of chromosomes is in metaphase. Here, we show that compaction instead peaks during late anaphase, just before telophase decompaction, and is independent of cleavage-furrow ingression.

To study chromosome compaction in intact cells we use a definition of compaction applicable to the limited resolution of live-cell fluorescence microscopy<sup>19</sup>: a change in the condensation or compaction of a chromosome is a change in its density. This can be measured in four-dimensional imaging experiments controlled for artefacts due to focus shifts and anisotropic resolution. Changes in the spatial distribution of chromosomes, or reductions in one of their dimensions, such as the length, are interpreted as compaction only if directly correlated with an increase in the density of the defined amount of chromatin. Furthermore, we distinguish between interchromosomal compaction, dependent on the proximity between two or more chromosomes, and intrachromosomal compaction, which occurs within a single chromatid.

To demonstrate intrachromosomal compaction, the density and lengths of fluorescently labelled single chromosomes and arm segments were measured using photoactivation and multicolour four-dimensional imaging throughout mitosis. These assays showed that the axial shortening of single chromosomes that began in mid-anaphase and finished during late anaphase led to the overall maximal compaction of chromatin in late anaphase (see Supplementary Information, Fig. S5). Chromatid segments of different initial lengths (~3.5–6.5 μm) in rat and human cells showed similar shortening kinetics (Figs 3 and 5), indicating that anaphase shortening is independent of chromosome size and evolutionarily conserved in mammals. In contrast, the apparent decompaction or increase in chromatin volume measured within 2 min of anaphase onset (Fig. 1b) is most likely not caused by intrachromosomal decompaction (for example, by stretching during sister segregation), as no significant changes in single chromatid length or density were detected during that period (Figs 2b, 3b). Instead, this apparent decompaction is most likely explained by the ongoing segregation of sister chromatids, which rapidly decreases the proximity between chromosomes and increases the amount of edges in the volume images.

How anaphase compaction by chromatid shortening is regulated at the molecular level is not known. We show that both the shortening and the correct localization of Aurora kinase depend on dynamic microtubules. Also, the activity of Aurora kinase is required for shortening. Therefore, we propose that localized Aurora B activity at the central spindle is necessary for anaphase chromatid shortening. Identifying mammalian Aurora B substrates required for anaphase compaction will be very interesting. Such experiments face the non-trivial challenge that the candidates may also be required for preceding mitotic stages, which could mask their role during the few minutes that mid-late anaphase lasts. Aurora B itself has important roles in chromatin phosphorylation and kinetochore attachment<sup>20</sup>, and the RNAi phenotype consequently also includes prometaphase and metaphase defects (ref. 18 and unpublished observations).

An alternative mechanism is that microtubule dynamics in mid-late anaphase could mechanically mediate chromatid compaction. Such forces could be generated and transmitted to chromosome arms by motors using microtubules as tracks. However, the sensitivity of anaphase compaction to taxol excludes the possibility that stabilized microtubules provide the tracks. Midspindle dynamics, through growth and/or shrinkage or tubulin flux, could also be coupled to chromosome arms through non-motor adaptors such as MAPs<sup>21</sup>, although the mechanical role of flux in mitosis is controversial<sup>22,23</sup>.

It is important to investigate the biological relevance of compacting-metaphase chromosomes even further during anaphase. Our study suggests two functions: first, in mammalian and other eukaryotic cells, long chromatids frequently protrude several micrometres from the focused mass of peri-centromeric chromatin after segregation. We show that anaphase chromatid compaction promotes the incorporation of such long chromosomes into a single daughter nucleus, with a smooth surface and normal architecture of chromosome territories. The consequence of inhibiting this anaphase compaction is a phenotype of severely multi-lobed daughter nuclei in G1. In this context, nuclear architecture can be important for gene regulation, as the localization of genes has been shown to influence their expression<sup>24,25</sup>. The increased contact surface of protruding chromatin lobes with the nuclear envelope may thus lead to misregulation when gene expression is being re-established in telophase-G1 (ref. 26; Neumann, B., F. M.-B. and J. E., unpublished observations).

Second, severe segregation errors, such as chromosome bridges, can lead to pathological damage of the genome<sup>2</sup>. Anaphase chromatid compaction could serve as an additional mechanism for the segregation of sister chromatids. It could help to resolve persistent chromosome bridges by functioning as a back-up force when the poleward movement of chromosomes is finished. This could explain why many segregation errors observed in anaphase cells with impaired condensin activity are eventually resolved<sup>9,27,28</sup>. Consistent with this view, we found a marked increase of persistent segregation defects in *condensin*-depleted cells after perturbation of chromatid shortening. This is reminiscent of the “NoCut” pathway recently identified in yeast, in which Aurora kinase activity is likewise necessary to protect unsegregated chromosomes from damage by cytokinesis<sup>29</sup>. Similarly, a delayed cytokinesis has also been observed in human primary and HeLa cells after segregation errors<sup>30</sup>.

In summary, we propose that anaphase compaction helps to establish the post-mitotic nuclear architecture and contributes to the rescue of segregation errors by shortening and removing chromosome arms from the cytokinesis plane, before the cleavage furrow can cut them. □

## METHODS

**DNA constructs, cell lines, inhibitor treatments and immunofluorescence microscopy.** EGFP-H2B was made by fusing the entire coding sequence of H2B 3' to EGFP (Clontech, Palo Alto, CA) generating a SGLRSRAQASNSAVDGTATM linker between the two proteins. Photoactivatable GFP-tagged H2B (H2B-PAGFP) was previously described<sup>31</sup>. mEGFP-α-tubulin was made by replacing EGFP by monomeric EGFP (mEGFP<sup>32</sup>) in EGFP-α-tubulin (Clontech). A monoclonal NRK cell line was generated that stably expresses EGFP-tagged core histone-2B (EGFP-H2B) as a fluorescent marker for chromatin (Fig. 1a). This line had a normal morphology and cell cycle compared with the maternal line, and the fluorescence localization through the cell cycle, as well as the redistribution after photobleaching (data not shown), was consistent with the literature<sup>31,33</sup>. Cell culture, transfection and generation of monoclonal NRK and HeLa cell lines stably expressing EGFP-H2B and EGFP-α-tubulin, and synchronization of NRK cells at the G1-S boundary with aphidicolin were performed according to standard

protocols<sup>8</sup>. Hoechst 33342 as a vital DNA counterstain was used at 100 ng·ml<sup>-1</sup>. Pre-warmed solutions of microtubule and kinase poisons, or equivalent solvent (DMSO) concentrations in mock experiments, were quickly but gently mixed with the medium, between two image acquisitions, on the microscope stage. Final concentrations: taxol (Sigma, St Louis, MO) and nocodazole (Calbiochem, Darmstadt, Germany), 20 µM; latrunculin (Calbiochem), 1 µM; hesperadin (Boehringer Ingelheim, Vienna, Austria), 30 µM. To match the IC<sub>50</sub> of hesperadin, ZM447439 (AstraZeneca, Alderley Park, UK) and roscovitine (Calbiochem) were used at 90 µM and 360 µM respectively. To interfere as little as possible with segregation and poleward migration, small molecule inhibitors were added when the last pairs of sister telomeres were segregated, ~2 min post-anaphase onset, except latrunculin, which was added 1 min post-anaphase onset to prevent cleavage furrow ingress. This did not interfere with segregation. Immunofluorescence microscopy was performed as previously described<sup>8</sup> after an 8 min incubation in either mock or inhibitor solution. The Aurora B antibody (BD Transduction Laboratories, Palo Alto, CA; anti-AIM1, clone 6) was visualized with Alexa 488-coupled goat anti-mouse antibodies (Molecular Probes, Eugene, OR).

**Confocal microscopy.** Images were acquired with customized LSM 510 or LSM 510 Meta confocal microscopes using a 63× Plan-Apochromat 1.4 N.A. oil objective (Carl Zeiss, Jena, Germany). NRK and HeLa cells expressing fluorescently tagged proteins were cultured in #1 LabTek chambers (Nalge Nunc, Rochester, NY) and imaged at 37 °C on the microscope stage. Potential phototoxicity effects were stringently controlled as previously described<sup>19</sup>, and the illumination levels used did not perturb the timing, length, kinetics or morphology of mitotic progression and exit.

**Four-dimensional imaging of mitotic cells.** To quantitate overall changes in large-scale chromosome compaction, all fluorescent chromatin was recorded through mitosis by three-dimensional time-lapse (four dimensional) automated confocal imaging, starting 4–5 h after release from a G1–S block with aphidicolin, before mitotic entry. For each nucleus, typical stacks of 512 × 512 pixels × 18 images were acquired for a maximum of 10 h (xyz resolution: 0.06 × 0.06 × 1.5 µm × 2–5 min, the highest possible allowing sufficient signal to noise without perturbing mitotic progression). Relative changes in the volume occupied by the fluorescent chromatin were quantified through mitosis using in-house developed macros in Heurisko 4.0 (Aeon, Hanau, Germany; see Supplementary Information, Methods). The inverse of this volume, represented by isosurface reconstructions in Fig. 1 (Amira 2.3; TGS, Bordeaux, France), gives a relative compaction measure when normalized to the interphase volume at 0 s. The spatial resolution of this assay is limited by the sampling and the resolution along the optical axis of ~0.8 µm. More detailed discussions on quantitative four-dimensional fluorescence imaging and image processing were previously published<sup>19,34</sup>.

**Measuring length and density of single-chromosome segments during mitosis.** Mitosis was recorded in live NRK cells by four-dimensional dual-colour imaging. Typical stacks of 256 × 256 pixels × 5–7 image planes, (xyz resolution 0.11 × 0.11 × 0.7–1.5 µm × 0.5–4 min) were acquired around the centre of the chromosomes of interest. Defined segments of single chromosomes were labelled and measured after selective photoactivation using one short pulse of a 405 or 413 nm laser line during chromosome congression, in NRK cells stably expressing photoactivatable GFP-tagged H2B (H2B-PAGFP). Length measurements were done interactively in single optical sections using the LSM 510 3.2 software (Carl Zeiss). Fluorescence intensity measurements were done in ImageJ (NIH; <http://rsb.info.nih.gov/ij/>). Total fluorescence intensity is the total amount of signal measured interactively within each entire photoactivated segment and reports on the total amount of photoactivated histones associated with the chromosome. Mean intensity is the total signal divided by the total number of pixels containing the signal and reports of the density of photoactivated histones. Chromatid segments were measured only if they were mostly contained in a combined optical field width half maximum of 1.5 µm or less over time, by controlling the remaining z-sections. This minimizes biases due to focus shifts and oblique orientations in z. Because illumination with 405 or 413 nm light in photoactivation and differential label imaging can perturb cell physiology, laser exposure was minimized to a level where toxic effects were not detected<sup>19</sup>. To further exclude a potential influence of phototoxicity on the compaction kinetics, the compaction was confirmed in 10 photoactivation experiments from prometaphase to G1, 30 photoactivation experiments from anaphase onset to G1 and 15 differential labelling experiments, but the shortening rates for anaphase were measured in cells expressing only EGFP-H2B, without 405 or 413 nm illumination.

**RNAi depletion of SMC2.** An established assay was used to deplete SMC2 (CAP-E), a component of both condensin I and II complexes, by RNAi, using HeLa (Kyoto) cells stably expressing H2B-EGFP, as previously described<sup>35</sup>, and transfection and imaging protocols, as well as validated Scrambled (Scr) and SMC2 siRNA oligonucleotides, also previously described<sup>9,35</sup>. Segregation defects were detected by the presence of fluorescent links between fluorescently labelled chromosomes, using high resolution confocal microscopy.

**Perturbing anaphase chromatid shortening with small molecule inhibitors.** To analyse the effects of the small molecule inhibitors in the shortening of chromatids, the inhibitors were added to cells expressing EGFP-tagged H2B ~2 min after anaphase onset, when segregation was complete (see Supplementary Information, Fig. S2 and Methods). In condensin-depleted cells, taxol was applied when the two chromatid masses were separated by at least the distance at which all chromatids are segregated in control small interfering RNA (siRNA)-treated cells, and when the poleward migration is mostly completed. This was ~1–3 min later than in control cells, probably due to the massive entanglement of chromosomes in early anaphase (Fig. 5a, c).

*Note: Supplementary Information is available on the Nature Cell Biology website.*

#### ACKNOWLEDGMENTS

MeCP2-EGFP was a kind gift from C. Cardoso. The anti-Aurora B antibody was a kind gift from J. M. Peters. We thank P. Lénart, M. Schuh, L. Sironi and J. M. Peters for fruitful discussions and critical reading of the manuscript. F.M.-B. was supported by the German Research Council (DFG EL 246/2-1/2) within the EuroDYNA European Science Foundation network (ESF 03-DYNA-F-29). D.G. was supported by a fellowship from the European Molecular Biology Organization (EMBO).

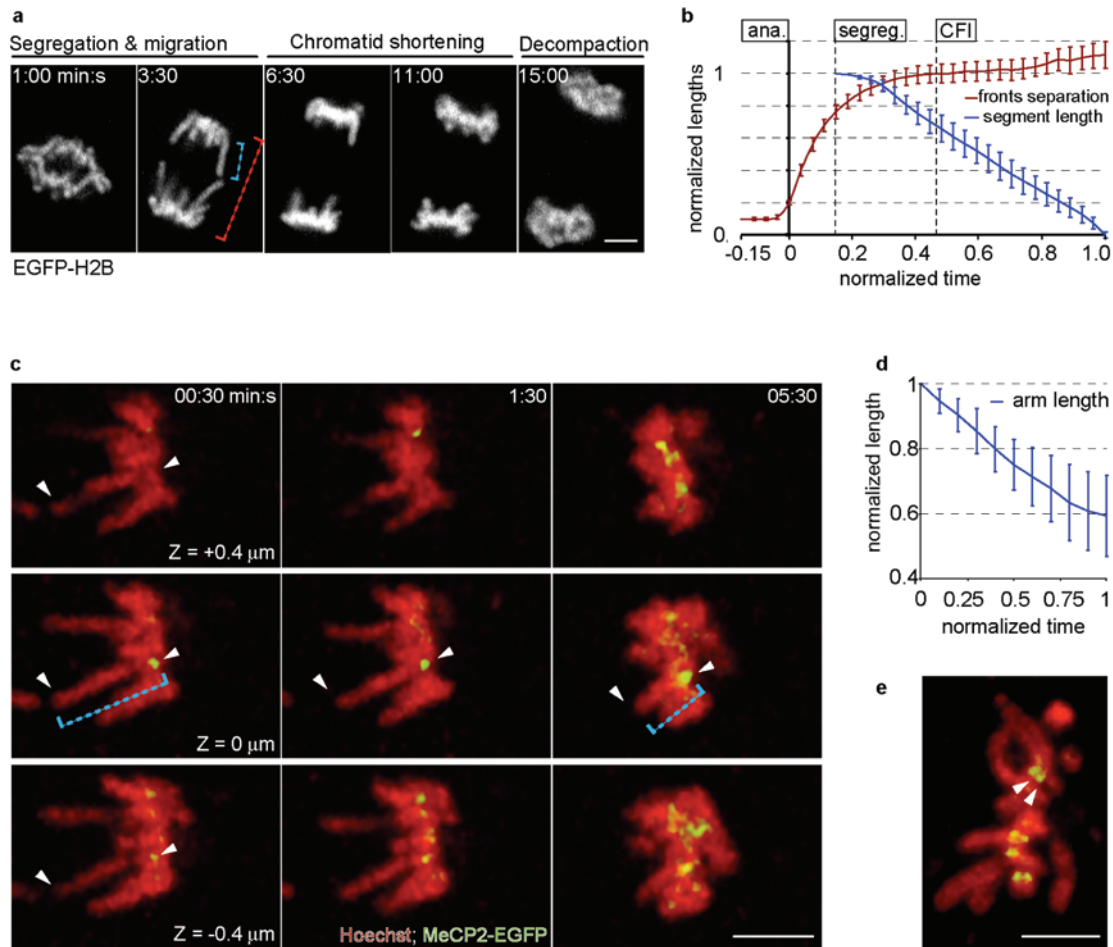
#### COMPETING FINANCIAL INTERESTS

The authors declare no competing financial interests.

Published online at <http://www.nature.com/naturecellbiology/>  
Reprints and permissions information is available online at <http://npg.nature.com/reprintsandpermissions/>

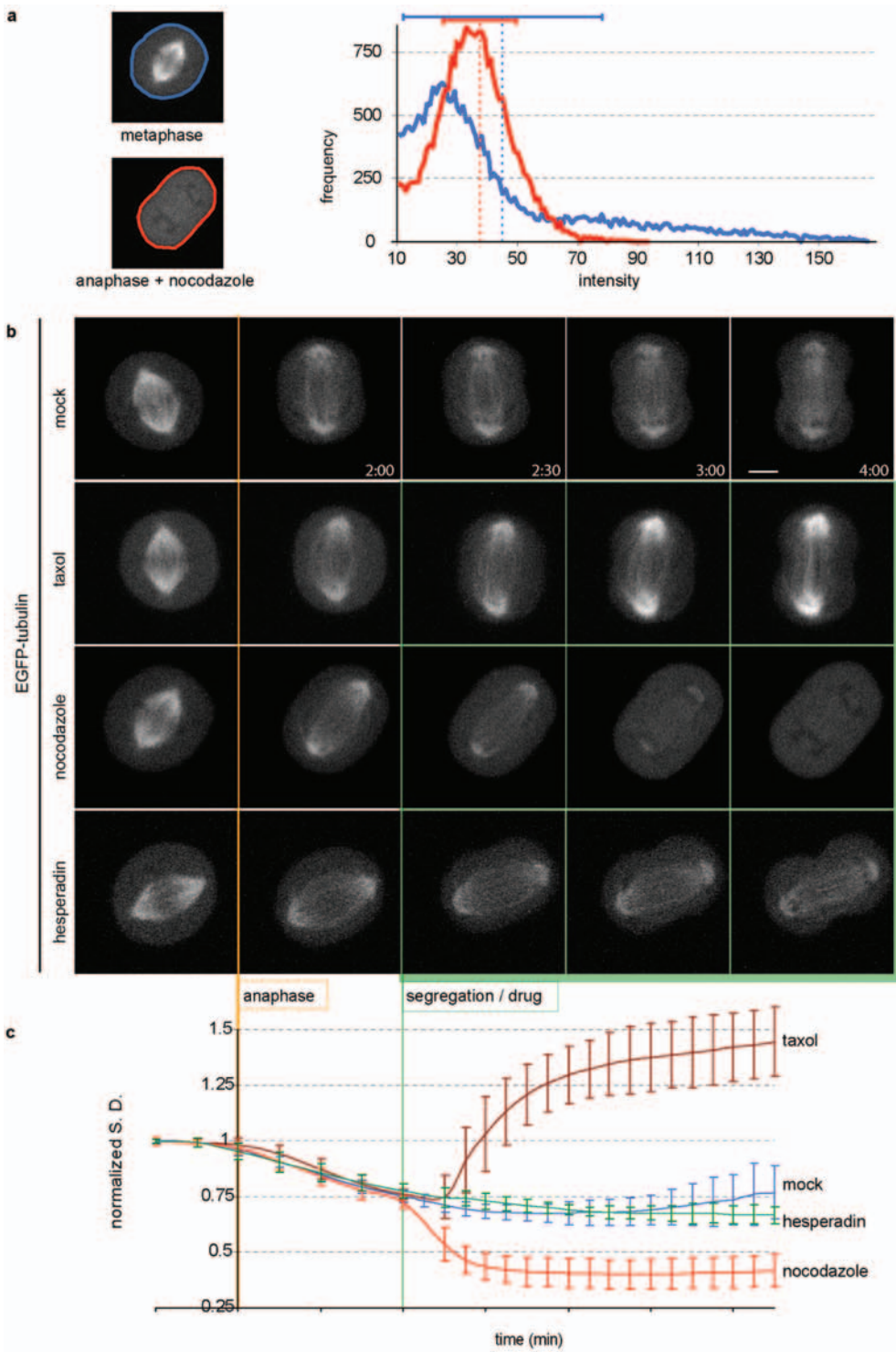
- Nasmyth, K. Segregating sister genomes: the molecular biology of chromosome separation. *Science* **297**, 559–565 (2002).
- Jallepalli, P. V. & Lengauer, C. Chromosome segregation and cancer: cutting through the mystery. *Nature Rev. Cancer* **1**, 109–117 (2001).
- Swedlow, J. R. & Hirano, T. The making of the mitotic chromosome: modern insights into classical questions. *Mol. Cell* **11**, 557–569 (2003).
- Swedlow, J. R., Sedat, J. W. & Agard, D. A. Multiple chromosomal populations of topoisomerase II detected *in vivo* by time-lapse, three-dimensional wide-field microscopy. *Cell* **73**, 97–108 (1993).
- Belmont, A. S., Braunfeld, M. B., Sedat, J. W. & Agard, D. A. Large-scale chromatin structural domains within mitotic and interphase chromosomes *in vivo* and *in vitro*. *Chromosoma* **98**, 129–143 (1989).
- Hiraka, Y., Minden, J. S., Swedlow, J. R., Sedat, J. W. & Agard, D. A. Focal points for chromosome condensation and decondensation revealed by three-dimensional *in vivo* time-lapse microscopy. *Nature* **342**, 293–296 (1989).
- Manders, E. M. *et al.* Four-dimensional imaging of chromatin dynamics during the assembly of the interphase nucleus. *Chromosome Res.* **11**, 537–547 (2003).
- Beaudouin, J., Gerlich, D., Daigle, N., Eils, R. & Ellenberg, J. Nuclear envelope breakdown proceeds by microtubule-induced tearing of the lamina. *Cell* **108**, 83–96 (2002).
- Gerlich, D., Hirota, T., Koch, B., Peters, J. M. & Ellenberg, J. Condensin I stabilizes chromosomes mechanically through a dynamic interaction in live cells. *Curr. Biol.* **16**, 333–344 (2006).
- D'Amours, D., Stegmeier, F. & Amon, A. Cdc14 and condensin control the dissolution of cohesin-independent chromosome linkages at repeated DNA. *Cell* **117**, 455–469 (2004).
- Lavoie, B. D., Hogan, E. & Koshland, D. *In vivo* requirements for rDNA chromosome condensation reveal two cell-cycle-regulated pathways for mitotic chromosome folding. *Genes Dev.* **18**, 76–87 (2004).
- Sullivan, M., Higuchi, T., Katis, V. L. & Uhlmann, F. Cdc14 phosphatase induces rDNA condensation and resolves cohesin-independent cohesion during budding yeast anaphase. *Cell* **117**, 471–482 (2004).
- Machin, F., Torres-Rosell, J., Jarmuz, A. & Aragon, L. Spindle-independent condensation-mediated segregation of yeast ribosomal DNA in late anaphase. *J. Cell Biol.* **168**, 209–219 (2005).
- Hauf, S. *et al.* The small molecule Hesperadin reveals a role for Aurora B in correcting kinetochore-microtubule attachment and in maintaining the spindle assembly checkpoint. *J. Cell Biol.* **161**, 281–294 (2003).
- Ditchfield, C. *et al.* Aurora B couples chromosome alignment with anaphase by targeting BubR1, Mad2, and Cenp-E to kinetochores. *J. Cell Biol.* **161**, 267–280 (2003).
- Bach, S. *et al.* Roscovitine targets, protein kinases and pyridoxal kinase. *J. Biol. Chem.* **280**, 31208–31219 (2005).

17. Vagnarelli, P. *et al.* Condensin and Repo-Man-PP1 co-operate in the regulation of chromosome architecture during mitosis. *Nature Cell Biol.* **8**, 1133–1142 (2006).
18. Neumann, B. *et al.* High-throughput RNAi screening by time-lapse imaging of live human cells. *Nature Methods* **3**, 385–390 (2006).
19. Mora-Bermudez, F. & Ellenberg, J. Measuring structural dynamics of chromosomes in living cells by fluorescence microscopy. *Methods* **41**, 158–167 (2007).
20. Ducat, D. & Zheng, Y. Aurora kinases in spindle assembly and chromosome segregation. *Exp. Cell Res.* **301**, 60–67 (2004).
21. Zhai, Y., Kronebusch, P. J. & Borisy, G. G. Kinetochore microtubule dynamics and the metaphase-anaphase transition. *J. Cell Biol.* **131**, 721–734 (1995).
22. Levesque, A. A. & Compton, D. A. The chromokinesin Kid is necessary for chromosome arm orientation and oscillation, but not congression, on mitotic spindles. *J. Cell Biol.* **154**, 1135–1146 (2001).
23. Ganem, N. J., Upton, K. & Compton, D. A. Efficient mitosis in human cells lacking poleward microtubule flux. *Curr. Biol.* **15**, 1827–1832 (2005).
24. Spector, D. L. The dynamics of chromosome organization and gene regulation. *Annu. Rev. Biochem.* **72**, 573–608 (2003).
25. Shaklai, S., Amariglio, N., Gideon, R. & Simon, A. Gene silencing at the nuclear periphery. *FEBS J.* **274**, 1383–1392 (2007).
26. Prasanth, K. V., Sacco-Bubulya, P. A., Prasanth, S. G. & Spector, D. L. Sequential entry of components of the gene expression machinery into daughter nuclei. *Mol. Biol. Cell* **14**, 1043–1057 (2003).
27. Bhat, M. A., Philp, A. V., Glover, D. M. & Bellen, H. J. Chromatid segregation at anaphase requires the barren product, a novel chromosome-associated protein that interacts with Topoisomerase II. *Cell* **87**, 1103–1114 (1996).
28. Hagstrom, K. A., Holmes, V. F., Cozzarelli, N. R. & Meyer, B. J. *C. elegans* condensin promotes mitotic chromosome architecture, centromere organization, and sister chromatid segregation during mitosis and meiosis. *Genes Dev.* **16**, 729–742 (2002).
29. Norden, C. *et al.* The NoCut pathway links completion of cytokinesis to spindle midzone function to prevent chromosome breakage. *Cell* **125**, 85–98 (2006).
30. Cimini, D., Fioravanti, D., Salmon, E. D. & Degrassi, F. Merotelic kinetochore orientation versus chromosome mono-orientation in the origin of lagging chromosomes in human primary cells. *J. Cell Sci.* **115**, 507–515 (2002).
31. Beaudouin, J., Mora-Bermudez, F., Klee, T., Daigle, N. & Ellenberg, J. Dissecting the contribution of diffusion and interactions to the mobility of nuclear proteins. *Biophys. J.* **90**, 1878–1894 (2006).
32. Snapp, E. L., Iida, T., Frescas, D., Lippincott-Schwartz, J. & Lilly, M. A. The fusome mediates intercellular endoplasmic reticulum connectivity in *Drosophila* ovarian cysts. *Mol. Biol. Cell* **15**, 4512–4521 (2004).
33. Kimura, H. & Cook, P. R. Kinetics of core histones in living human cells: little exchange of H3 and H4 and some rapid exchange of H2B. *J. Cell Biol.* **153**, 1341–1353 (2001).
34. Gerlich, D. & Ellenberg, J. 4D imaging to assay complex dynamics in live specimens. *Nature Cell Biol.* **9**, S14–S19 (2003).
35. Hirota, T., Gerlich, D., Koch, B., Ellenberg, J. & Peters, J. M. Distinct functions of condensin I and II in mitotic chromosome assembly. *J. Cell Sci.* **117**, 6435–6445 (2004).



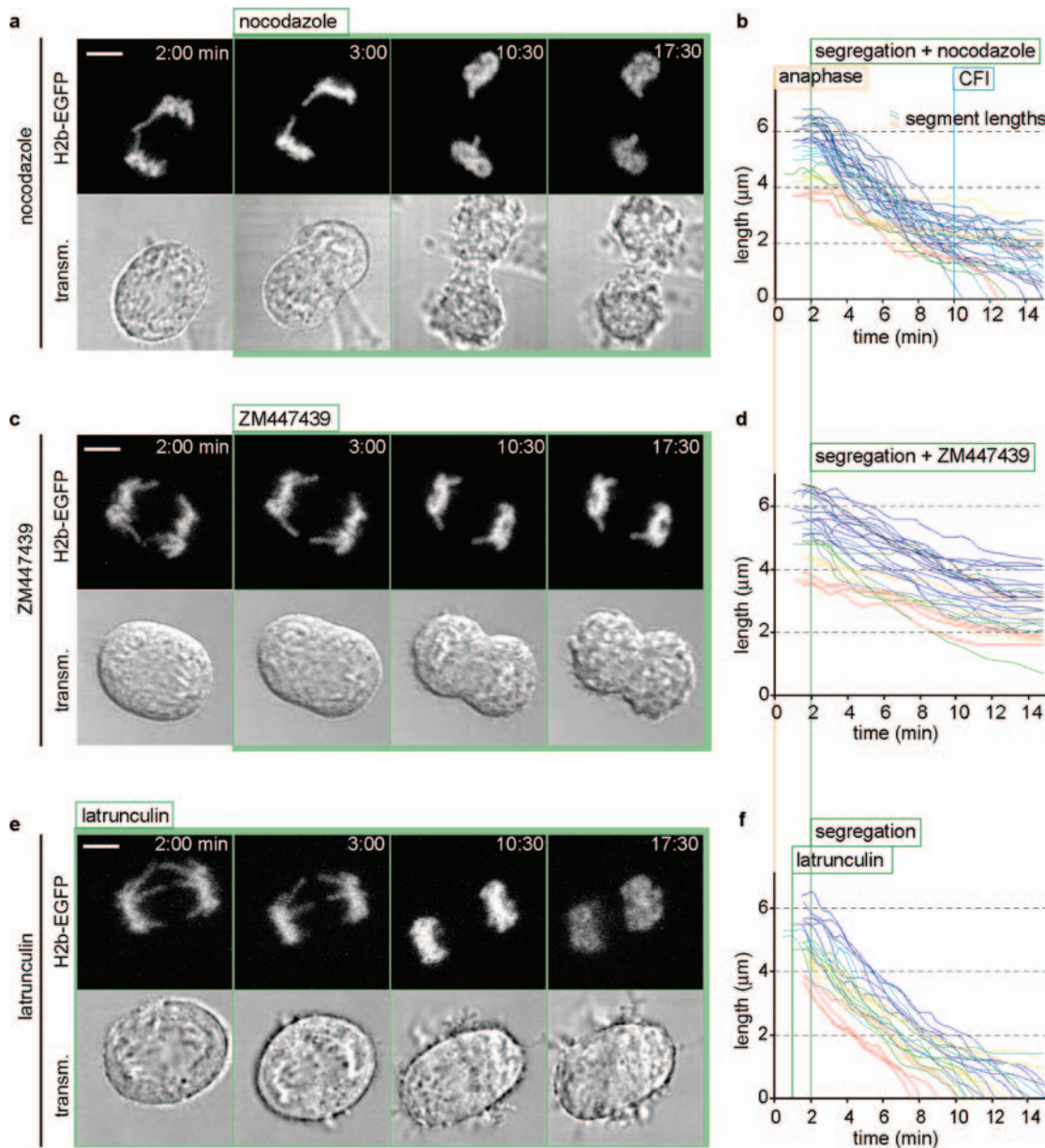
**Supplemental Information, Figure S1. Single chromatids shorten axially in anaphase and independently of the pole-pole separation of chromatin masses.** (a) Same NRK cell line expressing EGFP-H2B as in Fig. 1. The red dashed line at  $t = 3:30$  min measures the distance between migrating fronts of chromatin masses; The blue line measures the length of the chromatid arm protrusions. (b) Comparison of the mean normalized length of chromatid arm protrusions (blue; normalized time ( $n.t.$ ) = 0:00 is anaphase onset, 1:00 is no remaining protrusion) to the mean distance between the migrating fronts of the chromatin mass, formed by sub/centromeric regions (red), normalized to this distance when the cleavage furrow is fully ingressed (CFI), ( $n = 34$  chromatids in 15 independently-assayed cells; see Fig. 3A for single chromatid data in  $\mu\text{m}$ ). (c) NRK cells with chromosomes labelled by Hoechst (red) and pericentromeric heterochromatin labelled with MeCP2-EGFP (green). Middle row shows the pericentromeric region and corresponding chromatid arm in the same focal plane (arrow heads) for measurement (blue dotted line). The upper and bottom rows show the immediately 0.4  $\mu\text{m}$  above and below sections, showing that selected chromatid arms and their respective pericentromeric region stay together in focus and can be tracked through anaphase. (d) Mean length over time between the pericentromeric region and distal tip of chromosomes, normalized to this length shortly after segregation ( $n.t. = 0$  is  $\sim 3$  min post anaphase onset,  $n.t. = 1$  is when the length is shortest (6-13 min);  $n = 15$  chromatids from 9 cells in 6 independent experiments). (e) In a live metaphase, MeCP2-EGFP localizes to paired foci (arrow heads), typical for centromeric and pericentromeric markers (see also Supplementary Information, ref. 3). Bars = 5  $\mu\text{m}$ .

## SUPPLEMENTARY INFORMATION



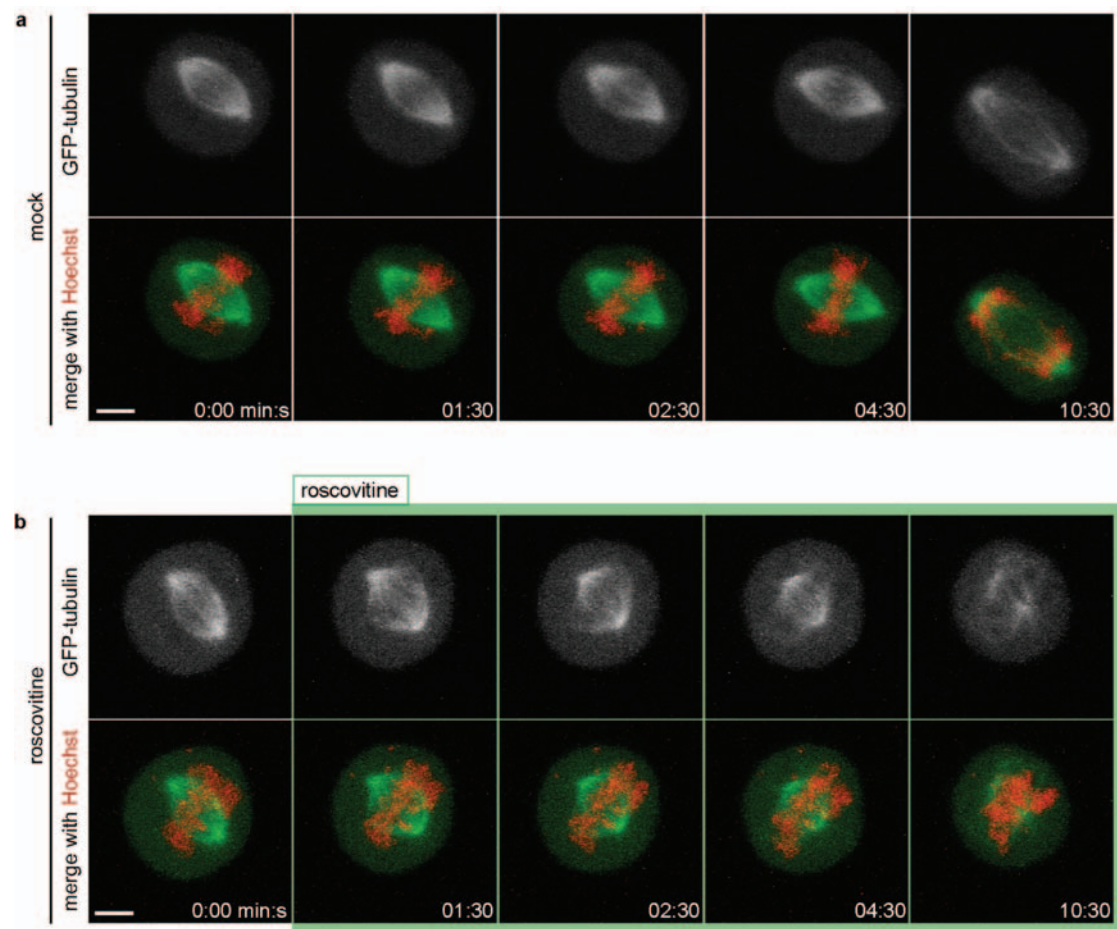
**Supplementary Information, Figure S2. Microtubule poisons acutely perturb anaphase microtubules within 2 min.**

(a) Distribution of tubulin fluorescence and histogram of pixel intensities in maximum intensity projections of monoclonal NRK cells stably expressing mEGFP-a-tubulin, in metaphase without drug treatment (upper panel) or anaphase after 2 min nocodazole treatment (lower panel). Dotted vertical lines indicate mean intensities, horizontal bars are standard deviations (SD). The SD was high in cells with structured microtubules and low in cells with mostly soluble tubulin after depolymerization (See Supplementary Information Methods). (b) Time-lapses from meta- to telophase of representative cells treated with taxol, nocodazole or hesperadin, ~2 min post-anaphase onset, when segregation was complete ( $n = 10$  for each treatment). In mocks, only pre-warmed medium with an equivalent concentration of solvent (DMSO) was added. (c) Normalized SDs from metaphase to anaphase. Bar = 5  $\mu$ m.

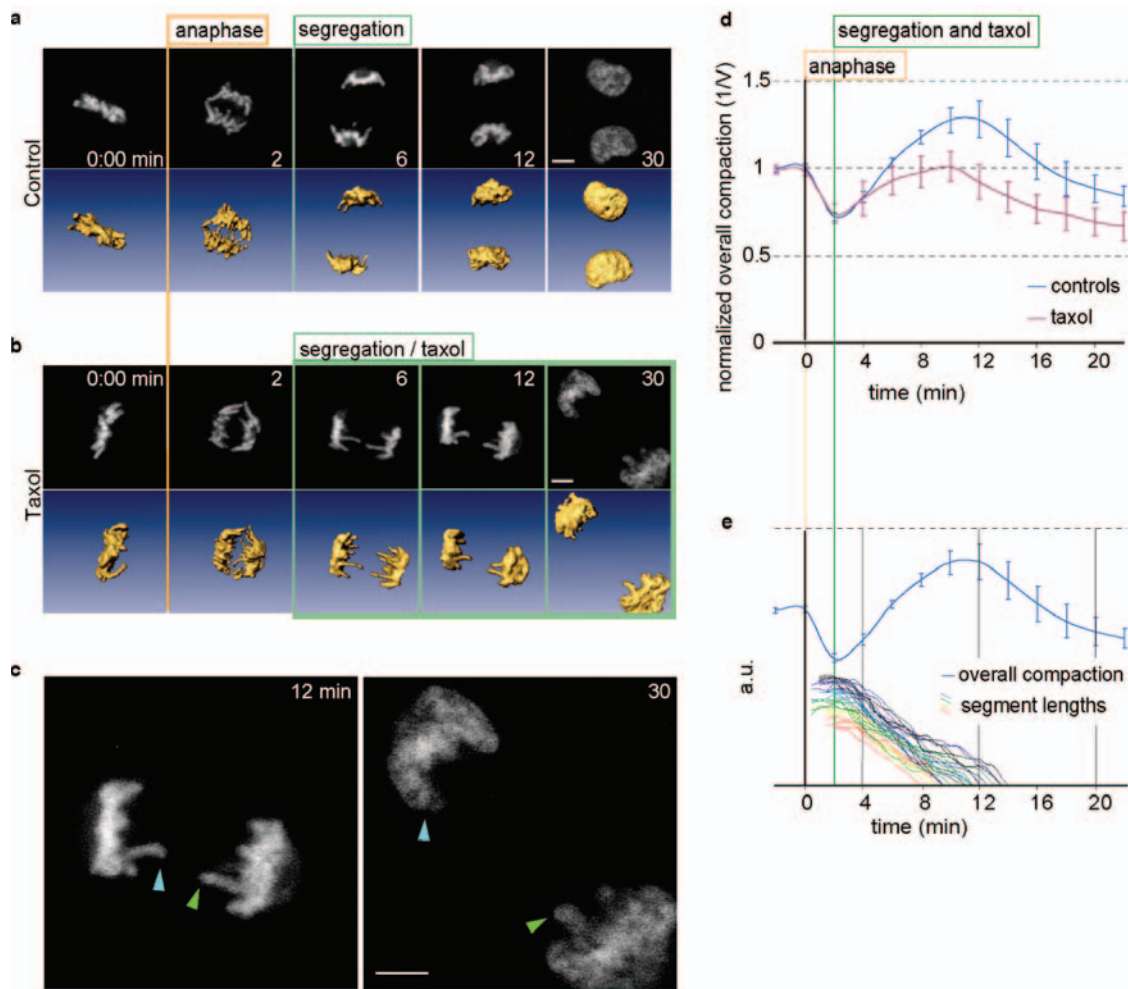


**Supplemental information, Figure S3. The microtubule depolymerizing drug nocodazole and the Aurora kinase inhibitor ZM447439 perturb axial arm shortening in anaphase, while the actin depolymerizing drug latrunculin A has no effect.** (a) Same as Fig. 3, but microtubules were acutely depolymerized with nocodazole immediately after segregation of all sister chromatids. CFI: full cleavage furrow ingression. (b) Quantitation of  $n = 36$  chromatid segment shortenings in 15 independently nocodazole-treated cells. Only 7 chromatids (19%) fully shorten within the normal 15 min. (c) Cell treated with the Aurora kinase inhibitor ZM447439. (d) Quantitation of  $n = 31$  chromatid segment shortenings in 10 independently ZM447439-treated cells. No chromatid fully shortens within 15 min. (e) Cell treated with the inhibitor of actin polymerization latrunculin A; note the absence of cleavage furrow ingression. (f) Quantitation of  $n = 30$  chromatid segment shortenings in 10 independently latrunculin-treated cells. 25 chromatids (83%) fully shorten within 15 min. Bars = 5  $\mu\text{m}$ .

## SUPPLEMENTARY INFORMATION



**Supplemental information, Figure S4. The CDK inhibitor roscovitine perturbs spindle formation within ~2.5 min and induces prometaphase arrest.** Representative examples of 6 independently mock-treated (a) and roscovitine-treated (b) cells. Roscovitine was added in mid-prometaphase, when a spindle was being formed but chromosomes were not yet congressed to the metaphase plate. The cell line stably expressing mEGFP-a-tubulin (green) is the same as in Supplementary Information, Fig. S2, counterstained with Hoechst (red). Bars = 5  $\mu$ m.



**Supplemental Information, Fig. S5. Large-scale anaphase compaction depends on dynamic microtubules and occurs simultaneously with single chromatid shortenings.** To test whether the compaction measured by volume changes is caused by the anaphase chromatid shortening, we investigated the taxol sensitivity of the large-scale compaction measured with the volumetric assay and compared the kinetics of volume decrease and arm shortening. (a-d) Same assay as described in Fig. 1, but at the highest temporal resolution compatible with normal mitosis between meta- and telophase (time lapse = 2 min). (a) Chromatin volume measurement in  $n = 8$  independently mock-treated cells, and (b) in  $n = 10$  independently taxol-treated cells. In addition to stopping chromosome shortening, taxol treatment reduced the large-scale anaphase chromatin compaction to a level similar to metaphase. (c) Zoom-in of the last two images of b, illustrating the multilobed daughter nuclei in taxol-treated cells. Each lobe was tracked back to an uncompacted chromatid (arrow heads). (d) Volume measurements of data illustrated in a & b. (e) Arm shortening data from Fig. 3b plotted in the same time scale as the volumetric data shown in d. Bars = 5  $\mu$ m.

#### Supplementary Movies

**Movie S1** Animation of the isosurface reconstruction set presented in Fig. 1a. The time lapse is ~5 min and the total time elapsed is 40 min, from prometaphase to telophase/G1.

**Movie S2** Photoactivation experiment similar to Fig. 2a, but initiated in mid anaphase, after the last pair of sister telomeres had separated. Time interval between frames is ~1.5 min and the total time elapsed is ~18 min, from mid-anaphase to telophase/G1. Representative example of  $n = 30$ . Consistent with our previous study<sup>6</sup>, chromosome segments marked by photoactivation kept their relative position and orientation throughout mitosis.

**Movie S3** Entire control time-lapse experiment set presented in Supplementary Information, Fig. S1a. The interval between frames is ~30 s. and the total time elapsed is 15 min, from metaphase to early telophase.

**Movie S4** Entire taxol time-lapse experiment presented in Fig. 3c. The interval between frames is ~30 s. and the total time elapsed is ~40 min, from metaphase to G1.